ACS APPLIED MATERIALS & INTERFACES

Research Article

www.acsami.org

Donor–Acceptor Copolymers Based on Thermally Cleavable Indigo, Isoindigo, and DPP Units: Synthesis, Field Effect Transistors, and Polymer Solar Cells

Chunchen Liu,[†] Sheng Dong,[†] Ping Cai,[†] Peng Liu,[†] Shengjian Liu,[†] Junwu Chen,[†] Feng Liu,[‡] Lei Ying,*[,†] Thomas P. Russell,*[,‡] Fei Huang,*[,†] and Yong Cao[†]

[†]Institute of Polymer Optoelectronic Materials & Devices, State Key Laboratory of Luminescent Materials and Devices, South China University of Technology, Guangzhou 510640, P. R. China

[‡]Department of Polymer Science and Engineering, University of Massachusetts, Amherst, Massachusetts 01003, United States

Supporting Information

ABSTRACT: A series of donor–acceptor type of π-conjugated copolymers based on *tert*-butoxycarbonyl (*t*-Boc) substituted indigo, isoindigo or diketopyrrolopyrrole as the acceptor unit and a benzodithiophene derivative as the donor unit was designed and synthesized. These copolymers can be readily dissolved in organic solvents and can produce uniform films by solution deposition. Thermal treatment of copolymer films at 200 °C for 10 min resulted in elimination of *t*-Boc side groups in nearly quantitative yield as suggested by thermogravimetric analysis and Fourier transform infrared spectroscopy. The elimination of the bulky *t*-Boc side groups resulted in the emergence of N–H···O═C hydrogen bonding interactions by virtue of the lactam structures of the indigo, isoindigo and diketopyrrolopyrrole units. Of particular interests is the distinctly increased field-effect mobility of these copolymers after thermal treatment, which may arise from the enhanced coplanarity and intermolecular ordering of the indigo, isoindigo or diketopyrrolopyrrole units after elimination of the bulky *t*-Boc side groups. These results demonstrate that the incorporation of latent side groups provides a viable strategy to construct conjugated polymers that can attain more ordered intermolecular stacking by simple thermal treatments. On the other hand, despite the thermal cleavage of *t*-Boc groups can also lead to increased ordering of polymer chains when blending with [6,6]-phenyl C71 butyric acid methyl ester, the photovoltaic performances of the resulting bulk heterojunction solar cells did not obviously increase due to the serious phase separation and coarsening of the film morphology.

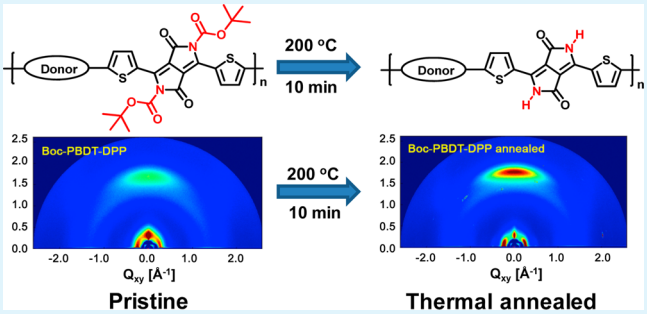

KEYWORDS: *conjugated polymers, thermal cleavage, hydrogen bonding, intermolecular ordering, organic field-effect transistor, polymer solar cell*

INTRODUCTION

Solution-processed conjugated polymers have attracted much attention because of their potential applications in various organic electronic devices, including polymeric light-emitting diodes (PLEDs), organic field-effect transistors (OFETs), and polymer solar cells (PSCs).[1−4] The film deposition of conjugated polymers typically needs spin-coating, inkjet printing, or blade coating, all of which require good solubility in a processing solvent. However, the rigid backbone of conjugated polymers retards their solubility in organic solvents, thereby necessitating the incorporation of solubilizing side groups, such as aliphatic, ether, or ester constituents. These side-chains, though, bearing sp^3-hybridized carbon atoms, decrease absorption, impede charge carrier transport, and negatively impact the photochemical stability. Much attention has been devoted to the rational design of side groups to address the trade-off between the conjugated architectures and solution processability, so that appropriate molecular ordered packing and charge carrier transport properties can be simultaneously reached without sacrificing the solubility.

An alternative strategy to attain solution processed polymer films is a precursor approach, wherein the solubilizing groups are introduced in during the polymerization to guarantee solubility and are then eliminated after deposition of polymer films.[5,6] This strategy has proven to be quite effective for the fabrication of poly(*p*-phenylene vinylene) (PPV) derivatives. Various conjugated polymers containing latent solubilizing side groups of Diels–Alder components,[7−9] tetrahydropyranyl groups,[10,11] silyl groups,[12,13] ester groups,[14−17] or ketal[18] substituents have been developed that allow for the deposition of thin films from solution followed by postprocessing elimination of such side chains.

Received: December 20, 2014
Accepted: April 13, 2015
Published: April 13, 2015

DOI: 10.1021/am5089956
ACS Appl. Mater. Interfaces 2015, 7, 9038−9051

Chart 1. Thermal Cleavage of *t*-Boc Side Chains from Copolymers

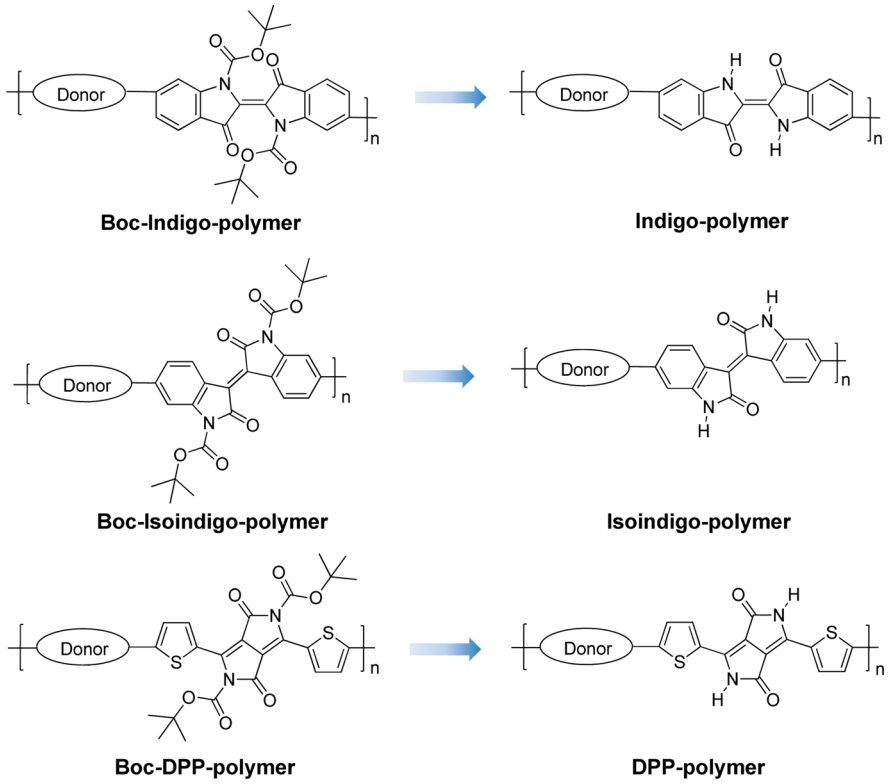

Recent progress in narrow band gap conjugated polymers has given rise to the development of the donor−acceptor (D−A)-type architectures, typically consisting of electron-rich (donor) and electron-deficient (acceptor) units alternating along the polymer main chain.[19,20] Among the reported acceptor moieties, much attention has been paid to indigo (I), isoindigo (II), and diketopyrrolopyrrole (DPP) derivatives, since conjugated polymers based on these electron-withdrawing units exhibited high device performance.[21−27] Of particular interests is the lactam structure in these moieties that can facilitate the formation of planar architectures and can potentially generate an N−H···O═C hydrogen bonding network after elimination of the latent side groups.[28] Since the ester group of *tert*-butoxycarbonyl (*t*-Boc) can act as an effective latent group in conjugated materials that can be easily removed at elevated temperature (~190 °C),[5,6,28] it would be interesting to construct solution-processed conjugated polymers by incorporating *t*-Boc groups as solubilizing latent substitutions in indigo, isoindigo, and DPP units.

Here, we describe a series of narrow band gap D−A type of conjugated polymers using *t*-Boc functionalized indigo, isoindigo, or DPP as the acceptor unit and a benzodithiophene (BDT) derivative as the donor unit.[29−32] All the polymers were readily dissolved in organic solvents and robust films were easily obtained. Additional thermal treatment on the prefabricated films at 200 °C led to the deprotection of *t*-Boc groups (Chart 1), resulting in enhanced molecular orientation along with magnitude significant enhancement in hole mobilities, as evaluated by field effect transistors. We also used these polymers as electron-donating materials to fabricated polymer solar cells by blending them with a fullerene derivative of [6,6]-phenyl C71 butyric acid methyl ester ($PC_{71}BM$). It was noted that despite the thermal cleavage of *t*-Boc groups can also lead to increased ordering of polymer chains in the blend films, the photovoltaic performances of the resulting bulk heterojunction solar cells did not obviously increase due to the serious phase separation and coarsening of the film morphology.

RESULTS AND DISCUSSION

Synthesis of Monomers and Polymers. The synthetic routes are shown in Scheme 1. By stirring the compound 6,6′-dibromoindigo (**1**),[33] 6,6′-dibromoisoindigo (**4**)[41] and 3,6-di(thiophen-2-yl)pyrrolo[3,4-*c*]pyrrole-1,4(2*H*,5*H*)-dione (**7**)[40] with di-*tert*-butyldicarbonate and dimethylaminopyridine (DMAP) in dichloromethane at room temperature (r.t.), we obtained *t*-butoxycarbonyl (*t*-Boc) protected intermediates 6,6′-dibromo-3,3′-dioxo-[2,2′-biindolinylidene]-1,1′-dicarboxylate (**2**), (*E*)-di-*tert*-butyl-6,6′-dibromo-2,2′-dioxo-[3,3′-biindolinylidene]-1,1′-dicarboxylate (**5**) and (*E*)-di-*tert*-butyl-6,6′-bis(5-bromothiophen-2-yl)-3,3′-dioxo-[2,2′-biindolinylidene]-1,1′-dicarboxylate (**8**) with good yields, respectively. The palladium-catalyzed Stille cross-coupling reaction of **2** and **5** with tributyl(thiophen-2-yl)stannane and tributyl(4-hexylthiophen-2-yl)stannane generates intermediates (*E*)-di-*tert*-butyl-3,3′-dioxo-6,6′-di(thiophen-2-yl)-[2,2′-biindolinylidene]-1,1′-dicarboxylate (**3**) and (*E*)-di-*tert*-butyl-6,6′-bis(4-hexylthiophen-2-yl)-2,2′-dioxo-[3,3′-biindolinylidene]-1,1′-dicarboxylate (**6**), respectively. Further bromination of **3**, **6** and **8** by *N*-bromosuccinimide (NBS) in tetrahydrofuran (THF) at room temperature gives the target dibromo-monomers (*E*)-di-*tert*-butyl-6,6′-bis(5-bromothiophen-2-yl)-3,3′-dioxo-[2,2′-biindolinylidene]-1,1′-dicarboxylate (**M1**), 6,6′-bis(5-bromo-4-hexylthiophen-2-yl)-2,2′-dioxo-[3,3′-biindolinylidene]-1,1′-dicarboxylate (**M2**), and 3,6-bis(5-bromothiophen-2-yl)-1,4-dioxopyrrolo[3,4-*c*]-pyrrole-2,5(1*H*,4*H*)-dicarboxylate (**M3**), respectively. The molecular structures of all monomers and

DOI: 10.1021/am5089956
ACS Appl. Mater. Interfaces 2015, 7, 9038−9051

Scheme 1. Synthetic Route for the Monomers and Copolymers[a]

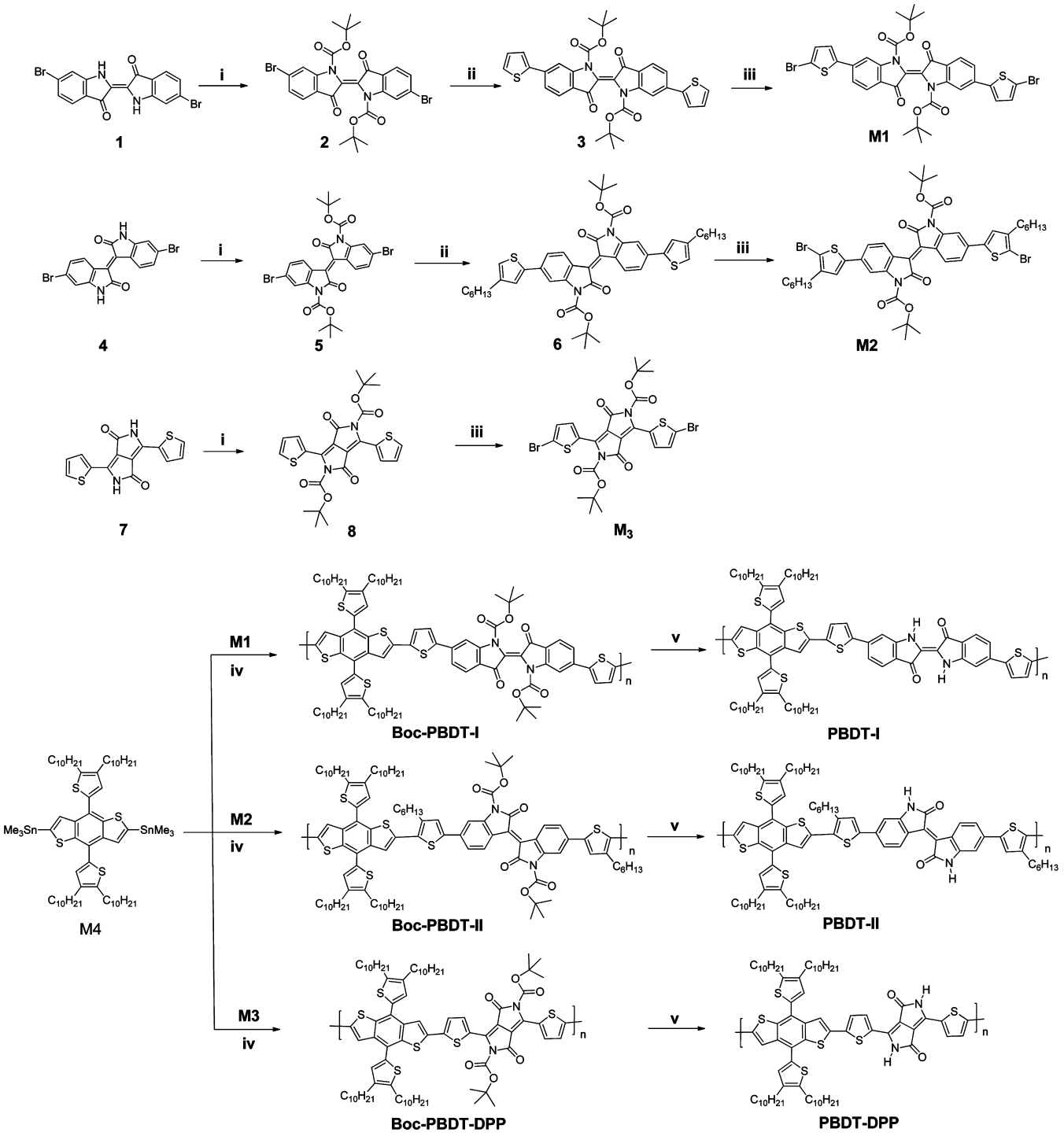

[a](i) DMAP, di-*tert*-butyl dicarbonate, CH_2Cl_2, r.t. 6 h; (ii) tributyl(thiophen-2-yl)stannane or (4-hexylthiophen-2-yl)trimethylstannane, $Pd_2(dba)_3$, P(*o*-Tol)$_3$, THF, 80 °C, 4 h; (iii) NBS, THF, r.t.; (iv) $Pd_2(dba)_3$, P(*o*-Tol)$_3$, toluene, 100 °C, 12 h; (v) thermally annealed at 200 °C, 10 min

intermediates are confirmed by ^{1}H and ^{13}C nuclear magnetic resonance (NMR) spectroscopy.

The palladium-catalyzed Stille copolymerization of dibromo-monomers **M1**, **M2**, and **M3** with bis-stannyl monomer (4,8-bis(4,5-didecylthiophen-2-yl)benzo-[1,2-b:4,5-*b*′]dithiophene-2,6-diyl)bis(trimethylstannane) (**M4**) generated targeting co-polymers, namely, Boc-PBDT-I, Boc-PBDT-II, and Boc-PBDT-DPP, respectively. All new copolymers were readily dissolved in THF, chloroform, chlorobenzene, and 1,2-dichlorobenzene and gave uniform thin films by solution-deposition. The molecular weights of copolymers were evaluated by gel permeation chromatography (GPC) measurement, which was carried out with THF as the eluent using linear polystyrene standards. The number-average molecular weight (M_n) of Boc-PBDT-I, Boc-PBDT-II, and Boc-PBDT-DPP was estimated to be 34.8, 24.3, and 33.7 kg mol^{-1} with polydispersity index (PDI) in the range of 2.11, 1.80, and 2.05, respectively.

DOI: 10.1021/am5089956
ACS Appl. Mater. Interfaces 2015, 7, 9038−9051

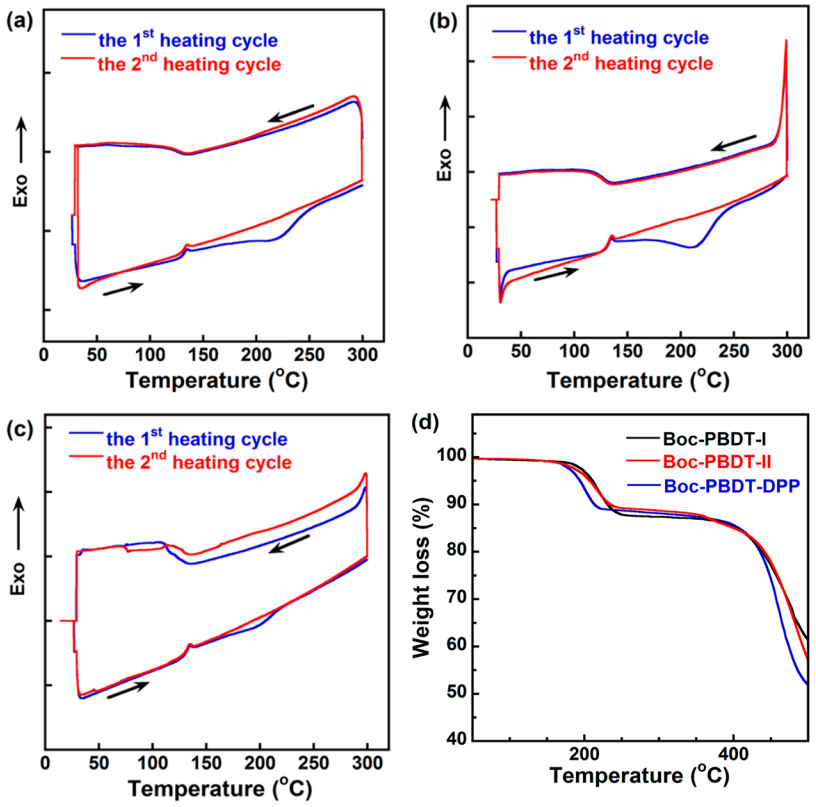

Figure 1. DSC characteristics of Boc-PBDT-I (a), Boc-PBDT-II (b), Boc-PBDT-DPP (c), and TGA characteristics (d) of precursors with heating rate of 10 °C min^{-1}.

Thermal Properties. Thermal behavior of these new polymers was evaluated by differential scanning chromatography (DSC) and thermogravimetric analysis (TGA). Initial DSC measurements at moderate heating rate from 25 to 140 °C, with the first heating and cooling cycle used to eliminate thermal history of samples (see Figure S1 in the Supporting Information). A distinct exothermal transition at ~135 °C was seen for all copolymers in the second heating cycle that can be attributed to the formation of ordered structures. However, no distinct glass transition could be identified for all the copolymers. Additional investigation of the deprotection of *t*-Boc side groups was carried out by increasing the scanning temperature to 300 °C (Figure 1a–c). An endothermic transition was seen in the temperature range of 180–230 °C, which is consistent with the thermal cleavage of the *t*-Boc groups. This broad endothermic transition disappeared in the following heating cycle, indicating a complete deprotection of *t*-Boc groups. It is worth noting that the cooling procedures exhibited a broad exothermic transition at ~120 °C for all copolymers, which may be attributed to the formation of ordered molecular stacking.

TGA showed a two-step thermal decomposition of these new copolymers. As shown in Figure 1d, the first weight loss occurred at ~190 °C aries from the elimination of *t*-Boc groups, corresponding to two equivalents of isobutene and CO_2.[5,6,28] The first weight loss corresponded to 13.4, 11.9, and 13.6 wt % for the Boc-PBDT-I, Boc-PBDT-II, and Boc-PBDT-DPP copolymers, respectively, in excellent agreement with the calculated value based on completed removal of the latent group (Table 1).[28] An additional step in the weight loss occurred at ~380 °C corresponding to the decomposition of the polymer backbone. The thermal characteristics of the copolymers are summarized in Table 1.

Table 1. Thermal Properties of Copolymers

copolymers	T_d^{1a} (°C)	T_d^{2a} (°C)	weight loss[b] (%)	weight loss[c] (%)
Boc-PBDT-I	184	380	13.0	13.4
Boc-PBDT-II	187	383	11.7	11.9
Boc-PBDT-DPP	181	387	14.2	13.6

[a] T_d^1 = Temperature of the first decomposition; T_d^2 = temperature of the second decomposition. [b] Theoretical weight loss of the *t*-Boc side groups. [c] Experimental weight loss of the *t*-Boc side groups.

FT-IR Spectroscopy. Fourier transform infrared (FT-IR) spectroscopy was used to monitor the thermal elimination of the *t*-Boc groups. The films were prepared by spin-coating from polymer solutions in 1,2-dichlorobenzene and were then thermally annealed at 200 °C for 10 min. As shown in Figure 2, the characteristic stretching vibration band of C═O at ~1700 cm^{-1} disappeared, and the characteristic band of C═O of the lactam moiety shifted to slightly small wave numbers. These observations clearly indicate the nearly complete deprotection of *t*-Boc side groups. In addition, it was noted that a relatively weak band emerged at ~3450 cm^{-1} after thermal treatment, which can be attributed to the interaction of N–H···O═C hydrogen bonding interactions of indigo, isoindigo and DPP units due to the lactam structures. Similar phenomena were also realized in the indigo, DPP based derivatives.[5,28]

Photophysical and Electrochemical Properties. Figure 3 shows the UV–vis absorption spectra of the copolymers in chloroform solution, as thin films, and after thermal treatment

DOI: 10.1021/am5089956
ACS Appl. Mater. Interfaces 2015, 7, 9038–9051

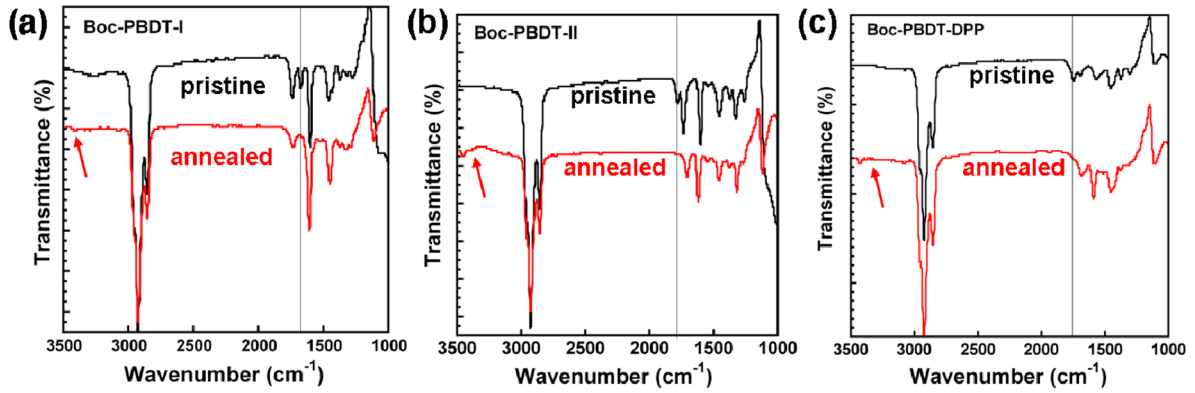

Figure 2. FT-IR spectra for the pristine films and after thermal treatment for copolymers: Boc-PBDT-I (a), Boc-PBDT-II (b), and Boc-PBDT-DPP (c).

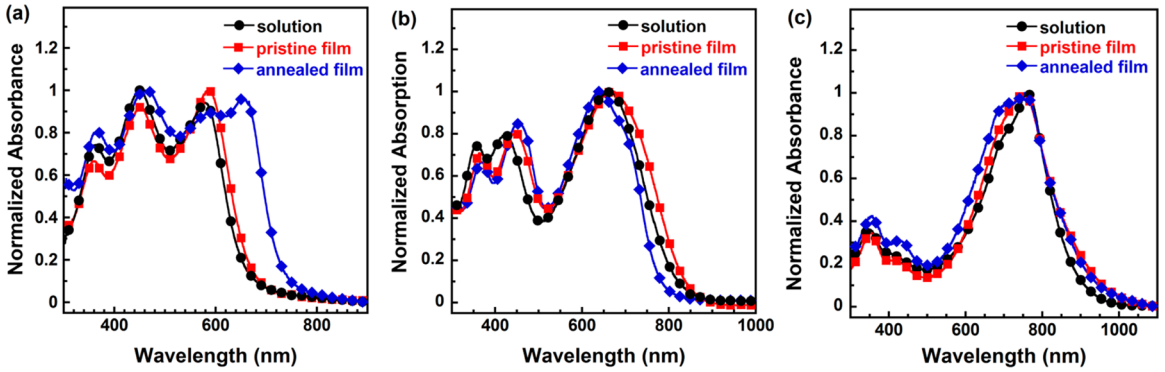

Figure 3. UV–vis absorption of copolymers in chloroform solution, as pristine thin films and after thermal treatment: Boc-PBDT-I (a), Boc-PBDT-II (b), and Boc-PBDT-DPP (c).

Table 2. Photophysical and Electrochemical Properties of Copolymers in Solutions and as Films

copolymers	conditions	λ_{max} solution	λ_{max} film	E_g^{opta} (eV)	E_{ox}^{onset} (V)	$E_{HOMO}{}^b$ (eV)	$E_{LUMO}{}^c$ (eV)
Boc-PBDT-I	pristine	452 577	453 585	1.88	1.17	−5.65	−3.77
	annealed		463 657	1.71	1.20	−5.68	−3.97
Boc-PBDT-II	pristine	424 662	448 676	1.48	0.95	−5.43	−3.95
	annealed		456 638	1.60	1.02	−5.50	−3.90
Boc-PBDT-DPP	pristine	351 767	353 767	1.40	0.90	−5.38	−3.98
	annealed		356 756	1.41	0.91	−5.39	−3.98

[a]Calculated from the onset of UV–vis absorption as pristine thin films. [b]$E_{HOMO} = -e(E_{OX} + 4.48)$ (eV). [c]$E_{LUMO} = E_g^{opt} + E_{HOMO}$.

at 200 °C for 10 min. All copolymers showed two absorption bands, where the dual-peaks below 500 nm can be attributed to the characteristic absorbance of $\pi-\pi^*$ of polymer backbones, while the low-energy absorbance, located in the region of 577–767 nm, can be attributed to the intramolecular charge transfer (ICT) effects corresponding the BDT unit and electron-withdrawing indigo, isoindigo and DPP units. The absorption profiles of pristine polymer films slightly red-shifted with respect to those in chloroform solutions, demonstrating the relatively weak aggregation in solid films, which is understandable, since the bulky *t*-Boc side groups may effectively hinder the formation of ordered stacking.[31,34,35]

Thermal treatment of the prefabricated thin films at 200 °C for 10 min led to variations in the absorption profiles. For Boc-PBDT-I (Figure 3a), a significant red-shift of ∼100 nm is seen after thermal treatment. We note that the elimination of the eletron-withdrawing *t*-Boc groups may lead to raised lowest unoccupied molecular orbital energy levels (E_{LUMO}) and hence increased band gaps; however, the formation of an intermolecular hydrogen bonding network, an increased planarity of the backbones after elimination of *t*-Boc side groups, or an enhanced intermolecular stacking, or a combination of all these factors can lead to pronounced red-shift of the absorption profile.[36] In this respect, the red-shift in the absorbance of the Boc-PBDT-I can be understood by the combined effects of the more pronounced enhancement of intermolecular interactions than the variation in the electronic structures of copolymers. In contrast, thermal treatment resulted in slightly hypsochromic shift of 38 and 10 nm of thin films of the copolymers Boc-PBDT-II and Boc-PBDT-DPP, respectively, relative to the pristine thin films. This hypsochromic shift can be correlated with the change in the frontier molecular orbitals of the copolymers after elimination of the *t*-Boc groups, or the less pronounced improvement in the intermolecular stacking of Boc-PBDT-II and Boc-PBDT-DPP than that of Boc-PBDT-I since the *t*-Boc groups are connected distal in isoindigo and DPP units while proximal in indigo unit.[34,35,37] The optical band gaps (E_g^{opt}) calculated from the

DOI: 10.1021/am5089956
ACS Appl. Mater. Interfaces 2015, 7, 9038–9051

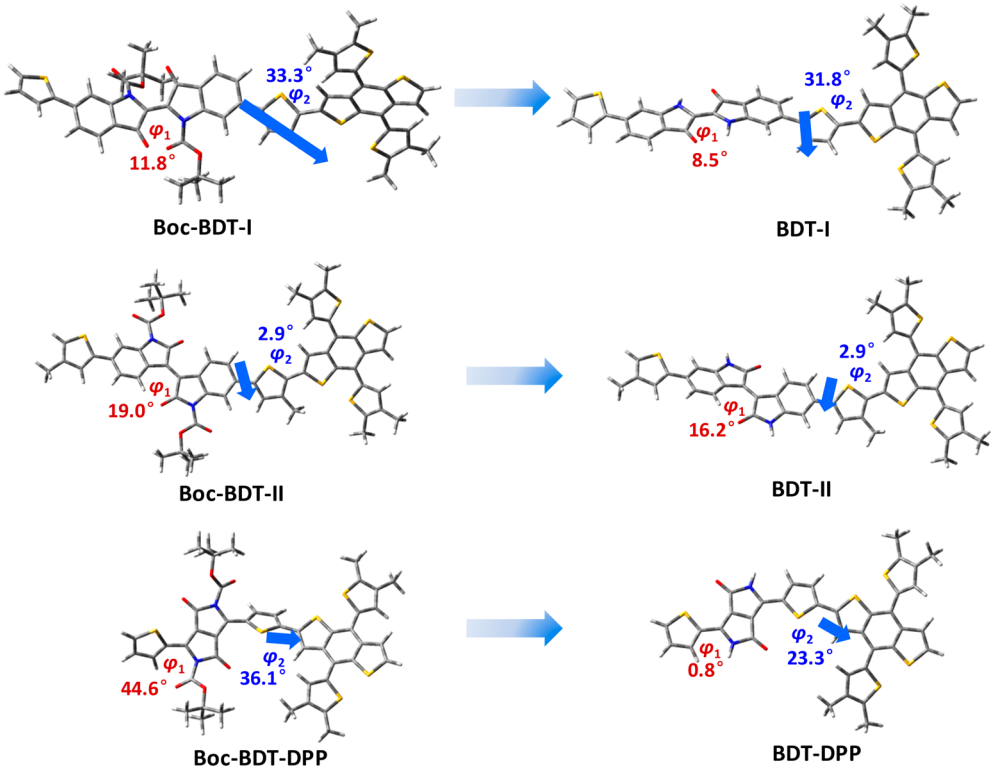

Figure 4. Calculated dipole moments and dihedral angles in copolymer repeat units. The arrows denote the magnitude and direction of the dipole moment of repeat units.

absorption onset were 1.88, 1.48, and 1.40 eV, for Boc-PBDT-I, Boc-PBDT-II and Boc-PBDT-DPP, respectively, which were changed to 1.71, 1.60, and 1.41 eV after thermal treatment, respectively. The detailed data of optophysical properties are summarized in Table 2.

Cyclic voltammetry (CV) measurements were used to determine the effect of thermal treatment on the frontier molecular orbitals of copolymers. The measurements were carried out under an inert atmosphere by using tetra-*n*-butylammoniumhexafluorophosphate (*n*-Bu_4NPF_6, 0.1 M in acetonitrile) as the supporting electrolyte with a glass carbon working electrode, a platinum wire counter electrode, and a saturated calomel electrode (SCE) as reference electrode. The potential of the ferrocene/ferrocenium (Fc/Fc^+) redox couple was measured as a standard. It is assumed that the redox potential of Fc/Fc^+ has an absolute energy level of −4.8 eV to vacuum.[38] Under the same experimental conditions, the onset potential of Fc/Fc^+ was measured to be 0.32 V with respect to the saturated calomel reference electrode. Therefore, the highest occupied molecular orbital energy levels (E_{HOMO}) of the copolymers were calculated as

$$E_{HOMO} = -e(E_{ox} + 4.48)\ (eV)$$

where the E_{ox} is the onset of the oxidation potential vs. SCE. The E_{HOMO} of the polymer precursors Boc-PBDT-I, Boc-PBDT-II, and Boc-PBDT-DPP were determined to be −5.65, −5.43, and −5.38 eV, which decreased slightly to −5.68, −5.50, and −5.39 eV, respectively, after thermal treatment. Since no reliable reduction characteristics were recorded in our measurements, the lowest unoccupied molecular orbital energy levels (E_{LUMO}) of copolymers were calculated from the difference between E_{HOMO} and E_g^{opt}, which was in the range of −3.77 to −3.98 eV. Despite the elimination of the electron-deficient *t*-Boc groups will lead to theoretically increased E_{LUMO}, however, we note that the thermal treatment of the pristine films caused distinctly decreased E_{LUMO} of Boc-PBDT-I, which can be understood by the combination of the slightly varied E_{HOMO} (from −5.65 to −5.68 eV) and obviously reduced optical band gap (from 1.88 to 1.71 eV). In contrast, the E_{HOMO} and E_g^{opt} of Boc-PBDT-II and Boc-PBDT-DPP did not show obvious variation, hence resulting in negligible variation of E_{LUMO}. The CV curves were illustrated in Supporting Information Figure S2 and detailed data were summarized in Table 2.

DFT Electronic Structure Calculation. To provide an insight into the disparity in molecular conformation of copolymers, theoretical calculation was carried out by using density functional theory (DFT) at the B3LYP/6-31G(d) basis with the Gaussian 09 package.[39] The repeat units of copolymers were utilized for the calculations, with the calculated torsional angles and dipole moments of the repeat units shown in Figure 4 and the relevant data summarized in Table 3. It was noted that the calculated HOMO of the repeat units mainly located in the BDT moiety, while the LUMO dominantly resided in the

Table 3. Dihedral Angles and Dipole Moments of Repeat Units by DFT Calculations

	dihedral angles (deg)		dipole moment (D)			
copolymer	φ_1	φ_2	*x*	*y*	*z*	total
Boc-BDT-I	11.8	33.3	−2.7991	−0.9512	−1.4851	3.31
BDT-I	8.5	31.8	0.1891	−1.4615	−0.0282	1.47
Boc-BDT-II	19.0	2.9	0.2988	1.2408	1.3229	1.84
BDT-II	16.2	2.9	0.1954	−0.9614	−1.3608	1.67
Boc-BDT-DPP	44.6	36.1	−1.0875	0.4032	1.0582	1.57
BDT-DPP	0.8	23.3	−0.9313	−0.5802	−0.4778	1.20

DOI: 10.1021/am5089956
ACS Appl. Mater. Interfaces 2015, 7, 9038−9051

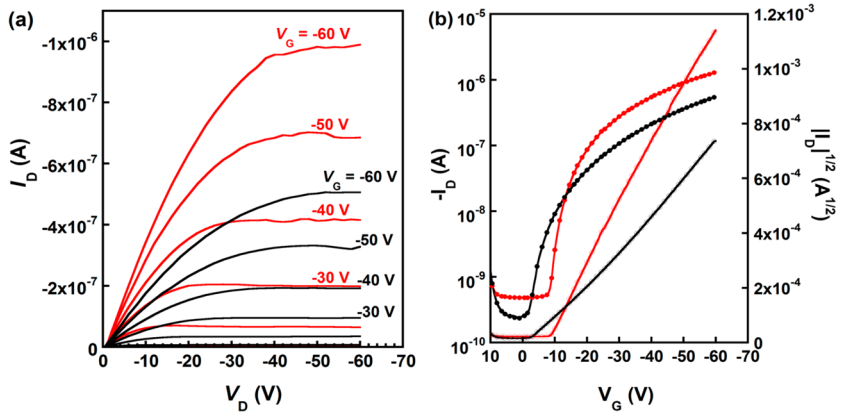

Figure 5. OFET output (a) and transfer characteristics (b) of Boc-PBDT-DPP. Black solid lines: Pristine film. Red solid line: Film after thermal treatment at 200 °C for 10 min.

electron-deficient indigo, isoindigo or DPP units (see Table S1 in the Supporting Information). In this respect, the elimination of the electron-withdrawing *t*-Boc unit did not significantly disturb the HOMO of the repeat units of copolymers, in good agreement with the trends seen in the CV measurements. In contrast, the LUMO of the copolymers increased slightly after removal of the electron-withdrawing *t*-Boc groups, which can be attributed to the reduced electron-affinity of the electron-withdrawing units. The dipole moments of the repeat units were also calculated to examine the effect of eliminating *t*-Boc on the electronic structures. The deprotection of *t*-Boc groups of the Boc-BDT-I showed the most pronounced effects on the dipole moment, which distinctly decreased for Boc-BDT-I (3.31 D), relative to BDT-I (1.47 D), along with a change in the direction, implying significant change of electronic structures of polymer backbone. The apparently changed dipole moment of Boc-BDT-I can be attributed to the unique molecular structure of the indigo unit, where the two indolinone moieties of the intrinsic indigo unit is not ideally conjugated, hence the elimination of the *t*-Boc groups can lead to more pronounced effects on electron delocalization along the repeating unit of BDT-I than those of BDT-II and BDT-DPP.

Since the molecular geometries can also be described by the intrinsic dihedral angles of the repeat units, we used the dihedral angles between the two fused rings of indigo (C−C−C−N), isoindigo (C−C−C−C), and between the thiophene and DPP unit (C−C−C−N), namely, φ_1, and the dihedral angles between the thiophene and BDT-derivative unit, namely φ_2, to examine the conformation of the backbones. It was noted that φ_1 was susceptible to the substituents on the *N*-atom of the acceptor units, which decreased slightly from 11.8° to 8.5° and from 19.0° to 16.2° for Boc-BDT-I and Boc-BDT-II, respectively, and a significant decrease from 44.6° to quasi-coplanar conformation of 0.8° for the repeat unit of Boc-BDT-DPP. In contrast, the variation of dihedral angles φ_2 is less pronounced relative to φ_1 upon the deprotection of the *t*-Boc groups. This indicates that the steric hindrance arising from the bulky *t*-Boc side groups can be effectively reduced by the elimination reaction, leading to improved coplanarity of the copolymer backbones. We note that the DFT calculations describe the molecules in vacuo, ignoring intermolecular interactions. Nonetheless, the theoretically enhanced coplanarity of backbone conformation after elimination of *t*-Boc groups may result in an improved intermolecular overlap integral that is beneficial for charge carrier mobility.

Organic Field Effect Transistor Performances. Bottom gate, top contact organic field effect transistors (OFETs) with the architecture of Si/SiO_2/poly(methyl methacrylate) (PMMA)/copolymer/Ag were fabricated to evaluate the influence of deprotection of *t*-Boc side groups on the charge carrier mobility. Our initial efforts on the fabrication of copolymer films focused on the use of the Si/SiO_2 wafer that was treated with a self-assemble monolayer of octadecyltrichlorosilane (OTS), however, uniform films cannot be formed on the top of such OTS-treated substrates. Hence, PMMA was used to modify the gate dielectric layer since uniform polymer films can be afforded.[40−43] The copolymer films were spin-coated from 1,2-dichlorobenzene solutions (10 mg mL^{-1}) for the control device, which was thermally treated at 200 °C for 10 min before the deposition of Ag for annealed devices. Despite Ag electrode is less efficient for good hole injection than that of Au electrode in the p-channel FET devices, herein we use Ag as the electrode due to the fact that it is more cost-effective and can be easily deposited on the top of the prefabricated polymer films, and it can effectively reveal the effects of thermal cleavage of the *t*-Boc groups on the variation of the FET moblities.[44−47] Figure 5 illustrated the output and transfer characteristics of OFETs, with Boc-PBDT-DPP as the semiconducting layer, were measured by sweeping the gate voltage (V_G) from −60 to 10 V under a source-drain voltage (V_D) of −60 V. At different V_G values, the drain current (I_D) of devices distinctly improved after thermal treatment. The hole mobility increased from 1.3×10^{-4} to 7.9×10^{-4} cm^2 V^{-1} s^{-1} after thermal elimination of the *t*-Boc side groups. Similar trends were also realized in devices based on the other two copolymers (see Figure S3 and Table S2 in the Supporting Information), which exhibited improved hole mobility of 3.2×10^{-5} and 9.1×10^{-5} cm^2 V^{-1} s^{-1} for Boc-PBDT-I and Boc-PBDT-II, respectively, after thermal treatment. The current on/off ratios (I_{on}/I_{off}) for all OFETs are in the range of 10^3−10^4. This suggests that the improved hole mobility after thermal elimination of *t*-Boc groups may be correlated with the improved coplanarity, that can lead to increased intermolecular stacking and improved charge carrier transport.

Bulk Heterojunction Polymer Solar Cells Performance. BHJ polymer solar cells were fabricated with an inverted device structure of ITO/PFN-OX/copolymer:$PC_{71}BM$/MoO_3/Al,[48,49,56] wherein the photoactive layer with [6,6]-phenyl C71

DOI: 10.1021/am5089956
ACS Appl. Mater. Interfaces 2015, 7, 9038−9051

butyric acid methyl ester ($PC_{71}BM$) as the acceptor, with the optimized weight ratio ofcopolymer:$PC_{71}BM$ of 1:4 for Boc-PBDT-I, and 1:3 for both Boc-PBDT-II and Boc-PBDT-DPP. A thin layer of poly[9,9-bis(6′-(*N*,*N*′-diethylamino)hexyl)-fluorene-*alt*-9,9-bis(3-ethyl(oxetane-3-ethyloxy)-hexyl)-fluorene] (PFN-OX, ∼5 nm) was spin-coated a top ITO as the electron transport layer since it can effectively reduce the work function of ITO and facilitate charge collection.[48,50] Elimination of *t*-Boc side groups was carried out by treating the prefabricated copolymer:$PC_{71}BM$ at 200 °C for 10 min. Device performances were measured under a simulated AM 1.5 G illumination of 100 mW cm^{-2}, with corresponding *J*−*V* characteristics shown in Figure 6 and photovoltaic parameters summarized in Table 4.

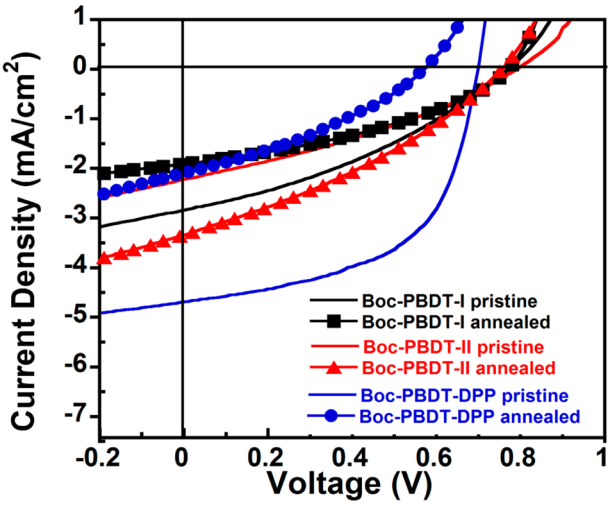

Figure 6. *J*−*V* characteristics of the polymer solar cells with active layer with or without thermal cleavage treatment at 200 °C for 10 min.

Table 4. Photovoltaic Parameters of Devices Measured under a Simulated AM 1.5G Illumination of 100 mW cm^{-2}

copolymer/ $PC_{71}BM$ (D/A)	conditions	D/A ratio	J_{sc} (mA cm^{-2})	V_{oc} (V)	FF (%)	PCE (%)
Boc-PBDT-I	pristine[a]	1:4	2.84	0.77	34.5	0.75
	annealed[b]	1:4	1.90	0.77	37.6	0.55
Boc-PBDT-II	pristine[a]	1:3	2.22	0.79	32.6	0.57
	annealed[b]	1:3	3.34	0.76	32.9	0.83
Boc-PBDT-DPP	pristine[a]	1:3	4.72	0.69	56.8	1.85
	annealed[b]	1:3	2.09	0.57	33.7	0.40

[a]Without thermal cleavage. [b]With thermal cleavage.

We note that all devices based on pristine copolymers as photoactive layer exhibited relatively high V_{OC} of 0.69−0.79 V, which was consistent with relatively deep E_{HOMO} of copolymers. However, the short circuit current (J_{SC}) of 2.22−4.72 mA cm^{-2} and fill factor of 32.6−56.8% were unexpectedly low, leading to moderate device performances with PCE of 0.57−1.85%. Thermal treatment of prefabricated photoactive layers led to a decrease in J_{SC} of Boc-PBDT-I and Boc-PBDT-DPP-based devices, while the J_{SC} of Boc-PBDT-II based devices increased slightly. This difference in J_{SC} might be correlated to the alternation of frontier orbital energy levels of polymer donors or the variation of microstructures of the copolymer:$PC_{71}BM$ films during the thermal annealing at relatively high temperature. The low PCEs of the devices may originate from a poor miscibility of the copolymers with $PC_{71}BM$, or roughening the film morphology that may impede collection of charge carriers.

Film Microstructure Analyses. To gain a picture of the correlation between molecular packing, charge carrier transport properties and photovoltaic properties, we investigated the morphology of the films before and after thermal treatment by grazing incidence X-ray diffraction (GIXD), atomic force microscopy (AFM) and transmission electron microscopy (TEM) (Figure 7, Figure 8 and Figure 9, respectively). The comparison of the GIXD patters of as-cast pure polymer films (Figure 7a−c) and thermally annealed films (Figure 7d-f) showed an improved order along with a distinctly reduced $\pi-\pi$ stacking distance (d_{010}). The d_{010} of pure polymer films was estimated to be in the range of 4.22−5.27 Å (Q = 1.19−1.49 $Å^{-1}$) for the as-cast films that decreased to 3.47−3.97 Å (Q = 1.58−1.81 $Å^{-1}$) after thermal cleavage. We note that the $\pi-\pi$ stacking planes primarily adopted a face-on orientation, since the (010) reflection is seen along Q_z. This orientation is, supposedly, not favorable for charge carrier transport, but since the charge carrier mobility is sensitive to the intermolecular overlap integrals,[41] the increase in the intensity of the sharp reflections for the thermally annealed films (Figure 7d−e) indicates a substantially improved intermolecular packing and higher mobilities.

In contrast, no distinct diffraction peak can be observed in the GIXD patterns of as cast copolymers:$PC_{71}BM$ blend films (Figure 7g−i), suggesting a random orientation of the polymer chains. In the GIXD patterns of the thermally annealed films, sharp (*n*00) reflections are seen along Q_z for BHJ films based on Boc-PBDT-II (Figure 7k) and Boc-PBDT-DPP (Figure 7l), indicating the largely enhanced ordering after thermal cleavage. It is also worth noting that an apparent (010) peak along Q_{xy} axis was observed for Boc-PBDT-DPP:$PC_{71}BM$ film. This, along with the (*n*00) peaks along Q_z, indicate an edge-on orientation after thermal annealing.

The effect of thermal treatment on the surface topographic features of copolymer films was examined by AFM. All samples were spin-casted from the polymer solutions in 1,2-dichlorobenzene followed by thermal treatment at the same conditions as devices fabrication. As shown in Figure 8, the Boc-PBDT-I films showed a relatively flat surface with nearly identical root-mean-square (RMS) values of ∼1.5 nm before and after thermal annealing. Thermal treatment of pure Boc-PBDT-II and Boc-PBDT-DPP films causes roughening with enhanced RMS values, along with the emergence of aggregates (size of about 170 ± 20 nm). In addition, one can observe the pronounced variation of films morphology of the copolymer:$PC_{71}BM$ blends (see Figure S5 in the Supporting Information), which also show aggregates and roughening after thermal treatment. Such distinctly roughening, with the significantly increased RMS values from 1.0 to 9.0 nm and from 1.3 to 45.9 nm for Boc-PBDT-I:$PC_{71}BM$ and Boc-PBDT-DPP:$PC_{71}BM$, respectively, can impede the charge carriers collection and lead to decreased device performances. In contrast, the RMS values of Boc-PBDT-II:$PC_{71}BM$ slightly decreased from 2.6 to 1.2 nm after thermal treatment. This smoothing in film morphology along with the reduced pinholes demonstrated the improved film morphology, which can lead to slightly increased PCE accordingly. Further examination of microstructures by polarized optical microscopy (POM) also showed the formation of large scale aggregates (see Figure S6 in the Supporting Information), which is consistent with the

DOI: 10.1021/am5089956
ACS Appl. Mater. Interfaces 2015, 7, 9038−9051

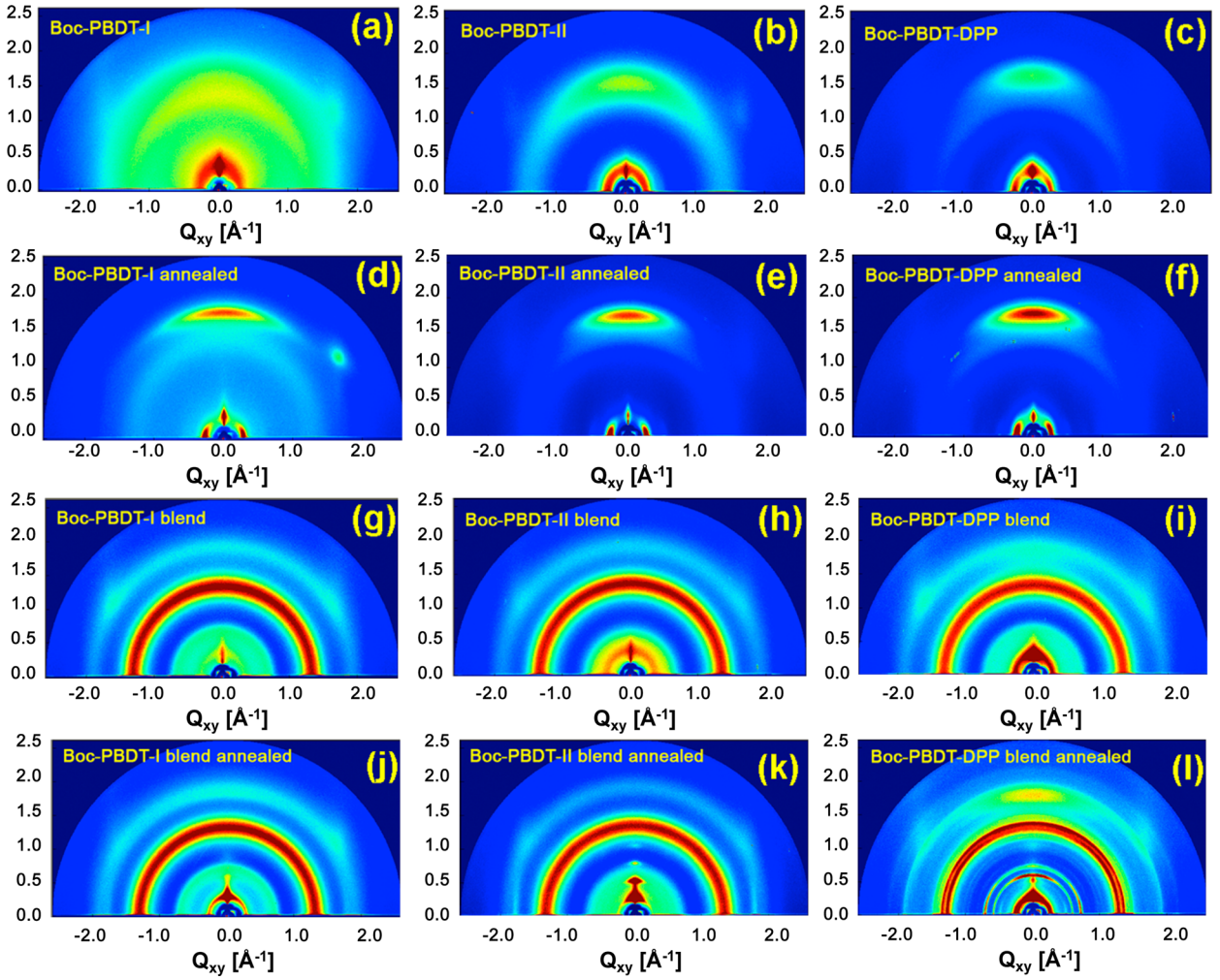

Figure 7. GIXD patterns of pristine polymers and blend films (copolymer:$PC_{71}BM$) before or after thermal cleavage of *t*-Boc groups. (a) Boc-PBDT-I pristine film; (b) Boc-PBDT-II pristine film; (c) Boc-PBDT-DPP pristine film; (d) Boc-PBDT-I annealed film; (e) Boc-PBDT-II annealed film; (f) Boc-PBDT-DPP annealed film; (g) Boc-PBDT-I: $PC_{71}BM$ pristine film; (h) Boc-PBDT-II: $PC_{71}BM$ pristine film; (i) Boc-PBDT-DPP: $PC_{71}BM$ pristine film; (j) Boc-PBDT-I: $PC_{71}BM$ annealed film; (k) Boc-PBDT-II: $PC_{71}BM$ annealed film; (l) Boc-PBDT-DPP: $PC_{71}BM$ annealed film.

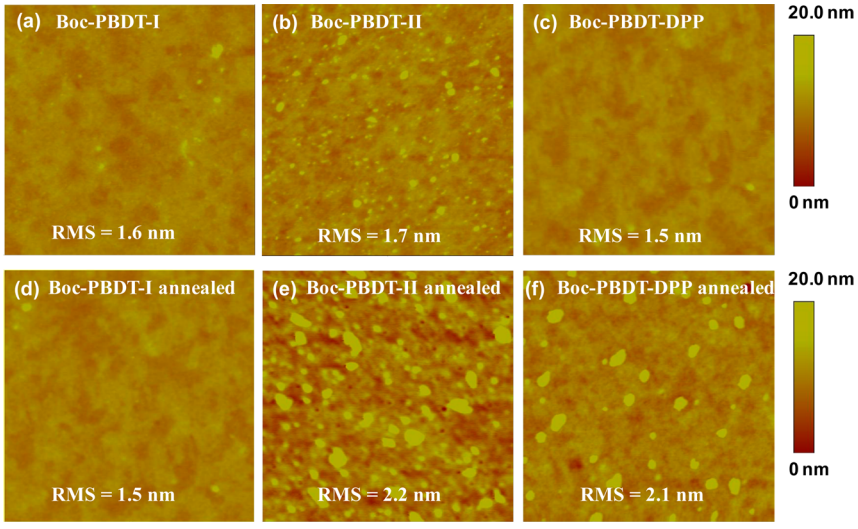

Figure 8. Tapping mode AFM images (5 × 5 μm) of polymer thin films as coated (a–c) and with thermal cleavage treatment by annealing at 200 °C for 10 min (d–f). (a, d) for Boc-PBDT-I; (b, e) for Boc-PBDT-II; (c), (f) for Boc-PBDT-DPP.

DOI: 10.1021/am5089956
ACS Appl. Mater. Interfaces 2015, 7, 9038–9051

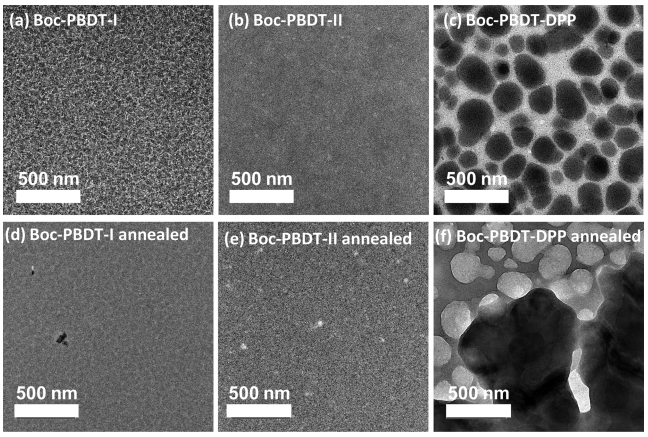

Figure 9. TEM images (the inset size of 500 nm) of polymer: $PC_{71}BM$ blend films as coated (a–c) and with thermal cleavage treatment by annealing at 200 °C for 10 min (d–f). (a) Boc-PBDT-I pristine blend film; (b) Boc-PBDT-II pristine blend film; (c) Boc-PBDT-DPP pristine blend film; (d) Boc-PBDT-I annealed blend film; (e) Boc-PBDT-II annealed blend film; (f) Boc-PBDT-DPP annealed blend film.

observed topographic features. We note that the morphology of blend films might be potentially improved by optimizing the heating speed during the thermal treatment, which can allow for the gradually evolution of the polymer backbone stacking to result in films high-quality that can reach high PCEs; however, this is beyond the scope of this study. Nonetheless, considering that the morphology of the copolymer:$PC_{71}BM$ blend films can play a key factor in the device performances of the polymer solar cells,[51−53] our future work will focus on improving PCEs by optimizing the morphology of photoactive layers through incorporating solvent additives, annealing the blend films at various heating speed, and so forth.

To clearly identify the domain change of $PC_{71}BM$ in the polymer:$PC_{71}BM$ blend films after thermal annealing treatment at 200 °C for 10 min, the transmission electron microscopy (TEM) characterization was conducted. As shown in Figure 9 and Supporting Information Figure S7, no obvious aggregation of $PC_{71}BM$ can be observed in the blend films of Boc-PBDT-I:$PC_{71}BM$ and Boc-PBDT-II:$PC_{71}BM$ (Figure 9a and 9b, respectively), but serious aggregations of $PC_{71}BM$ with size of about 50−100 nm was observed in blend film of Boc-PBDT-DPP:$PC_{71}BM$ (Figure 9c). After thermal treatment at 200 °C for 10 min, no distinct crystallization can be realized in the blend films of Boc-PBDT-I:$PC_{71}BM$ and Boc-PBDT-II:$PC_{71}BM$ (Figure 9d and 9e, respectively), while the Boc-PBDT-DPP:$PC_{71}BM$ film showed apparent copolymer crystallization domains along with the formation of extraordinarily large $PC_{71}BM$ aggregations (Figure 9f). We note that such unexpected severe phase separation is harmful for charge carrier transportation in the bulk heterojunction films, which can therefore lead to relatively low PCE of the resulting copolymers.

CONCLUSION

In summary, a series of narrow band gap conjugated polymers comprising *tert*-butoxycarbonyl (*t*-Boc) substituted indigo, isoindigo or diketopyrrolopyrrole as the acceptor moiety and a benzodithiophene derivative as donor moiety were designed and synthesized. Thermal treatment of the prefabricated copolymer films at 200 °C for 10 min leads to the elimination of *t*-Boc side groups in nearly quantitative yield along with the potentially formed hydrogen-bonding network, as indicated by thermogravimetric analysis and Fourier transform spectroscopy. Theoretical calculation by density functional theory implied that the elimination of bulky *t*-Boc side groups yields enhanced intrinsic coplanarity of repeat units of copolymers. Of particular interest is the distinctly improved hole mobility of all copolymers after the elimination of *t*-Boc side groups as measured by field effect transistors. Ordered packing microstructures for both pure copolymer films and copolymer:$PC_{71}BM$ blend films were realized after thermal removal of *t*-Boc side groups. These observations highlight the potential advantages of constructing solution-processed conjugated copolymers consisting latent thermally removal groups, which can be a promising strategy to reach enhanced charge carrier mobility along with more ordered microstructure packing as thin solid films.

EXPERIMENTAL SECTION

Materials. All reagents and solvents, unless otherwise specified, were obtained from Aldrich and Alfa-Aesar Chemical Co. and were used as received. Tetrahydrofuran was freshly distilled from sodium/benzophone before use. Compound 6,6′-dibromoindigo (**1**),[26] 6,6′-dibromoisoindigo (**4**),[42] 3,6-di(thiophen-2-yl)pyrrolo[3,4-*c*]pyrrole-1,4(2*H*,5*H*)-dione (**7**), and (4,8-bis(4,5-didecylthiophen-2-yl)benzo-[1,2-b:4,5-*b*′]dithiophene-2,6-diyl)bis(trimethylstannane) (**M4**) were synthesized according to the reported procedures.[54,55,43] Poly[9,9-bis(6′-(*N*,*N*′-diethylamino)hexyl)-fluorene-*alt*-9,9-bis(3-ethyl(oxetane-3-ethyloxy)-hexyl)-fluorene] (PFN-OX) was synthesized according to the previously reported methods.[36]

Synthesis of Monomers. *Synthesis of (E)-Di-tert-butyl 6,6′-dibromo-3,3′-dioxo-[2,2′-biindolinylidene]-1,1′-dicarboxylate (**2**).* In a three-necked, oven-dried 100 mL round-bottom flask, 6,6′-dibromoindigo (**1**) (1.26 g, 3 mmol) was dissolved in 30 mL of dichloromethane and the resulting solution was purged with argon for 20 min. Dimethylaminopyridine (37 mg, 0.3 mmol) was added, and the reaction mixture was stirred for 30 min under argon at room temperature. Di-*tert*-butyl-dicarbonate (1.44 g, 6.6 mmol) was then added in one portion and the mixture was stirred at room temperature for 24 h. Then the reaction mixture was filtered and a reddish solid was obtained, which was washed thoroughly by methanol. The crude product was purified by flash chromatography using dichloromethane as eluent. After organic solvent was removed in vacuo, the target compound was afforded as a red powder. (1.44 g, 77%). ^{1}H NMR ($CDCl_3$, 600 MHz): 8.25 (s, 1H), 7.62 (d, J = 8,34 Hz, 1H), 7.36 (m, J = 9.63 Hz, 1H), 1.61 (s, 9H). ^{13}C NMR ($CDCl_3$, 600 MHz): 182.39, 149.49, 149.41, 131.08, 127.77, 125.01, 121.67, 120.19, 85.25, 28.06. Anal. Calcd for $C_{26}H_{24}Br_2N_2O_6$: C, 50.34; H, 3.90; N, 4.52. Found: C, 50.61; H, 3.69; N, 4.53.

*Synthesis of (E)-Di-tert-butyl 3,3′-dioxo-6,6′-di(thiophen-2-yl)-[2,2′-biindolinylidene]-1,1′-dicarboxylate (**3**).* To a round-bottom flask, compound **2** (0.63 g, 1.02 mmol), tributyl(thiophen-2-yl)stannane (0.95 g, 2.55 mmol) and anhydrous tetrahydrofuran (THF, 30 mL) were added, and the mixture was bubbled with nitrogen, tris(dibenzylideneacetone)dipalladium(0) ($Pd_2(dba)_3$, 5 mg), and tri(*o*-tolyl)phosphine ($P(o\text{-tol})_3$, 10 mg) were added in one portion. The solution was bubbled with nitrogen for another 20 min. The mixture was stirred at 80 °C under nitrogen for 4 h. Then the mixture was cooled to room temperature and poured into water. The organic phase was extracted by dichloromethane, and then washed with water, dried over anhydrous magnesium sulfate. After removal of the solvent under reduced pressure, the solid were purified by silica chromatography with dichloromethane as the eluent to give the final compound as a brownish solid (0.45 g, 72%). ^{1}H NMR ($CDCl_3$, 600 MHz): 8.31 (s, 1H), 7.77 (d, J = 7.91 Hz, 1H), 7.51 (d, J = 3.38 Hz, 1H), 7.47 (d, J = 9.59 Hz, 1H), 7.41 (d, J = 5.11 Hz, 1H), 7.15 (d, J = 8.49 Hz, 1H), 1.68 (s, 9H). ^{13}C NMR ($CDCl_3$, 600 MHz): 182.65, 149.91, 149.59, 143.44, 141.66, 128.56, 127.22, 125.44, 124.71,

DOI: 10.1021/am5089956
ACS Appl. Mater. Interfaces 2015, 7, 9038−9051

121.86, 121.66, 113.50, 84.68, 28.22. Anal. Calcd for $C_{34}H_{30}N_2O_6S_2$: C, 64.16; H, 4.82; N, 4.47; S, 10.23. Found: C, 63.92;H, 5.02; N, 4.43; S, 10.26.

*Synthesis of (E)-Di-tert-butyl-6,6′-dibromo-2,2′-dioxo-[3,3′-biindolinylidene]-1,1′-dicarboxylate (**5**).* Compound **5** was synthesized following the same procedure as that of compound **2** by using 6,6′-dibromoisoindigo (**4**) as the instead of compound **1** as the starting material.(1.59 g, 85%). ^{1}H NMR ($CDCl_3$, 600 MHz): 8.84 (d, J = 8.71 Hz, 1H), 8.06 (d, J = 1.81 Hz, 1H), 7.32 (m, J = 10.56 Hz, 1H), 1.67 (s, 9H). ^{13}C NMR ($CDCl_3$, 600 MHz): 165.38, 148.38, 141.95, 131.79, 130.19, 127.78, 127.31, 120.48, 117.89, 85.54, 28.10. Anal. Calcd for $C_{26}H_{24}Br_2N_2O_6$: C, 50.34; H, 3.90; N, 4.52. Found: C, 50.30; H, 3.80; N, 4.62.

*Synthesis of (E)-Di-tert-butyl 6,6′-Bis(4-hexylthiophen-2-yl)-2,2′-dioxo-[3,3′-biindolinylidene]-1,1′-dicarboxylate (**6**).* Compound **6** was synthesized according to the same method as that in the synthesis of compound **3** except that tributyl(4-hexylthiophen-2-yl)stannane was used instead of tributyl(thiophen-2-yl)stannane (1.27 g, 79%). ^{1}H NMR ($CDCl_3$, 600 MHz): 8.95 (d, J = 8.56 Hz, 1H), 8.07 (s, 1H), 7.40 (d, J = 10.03 Hz, 1H), 7.31 (s, 1H), 6.96 (s, 1H), 2.64 (t, J = 15.37 Hz, 2H), 1.65 (s, 9H), 1.64 (m, J = 30.12 Hz, 2H), 1.33 (t, J = 14.22 Hz, 2H), 1.32 (m, J = 6.75 Hz, 4H), 0.90 (t, J = 13.51 Hz, 3H); ^{13}C NMR ($CDCl_3$, 600 MHz): 166.36, 148.69, 144.88, 143.54, 141.60, 138.75, 129.57, 126.24, 121.53, 121.10, 120.87, 111.05, 84.90, 31.69, 30.60, 30.42, 29.01, 28.23, 22.62, 14.11. Anal. Calcd for $C_{46}H_{54}N_2O_6S_2$: C, 69.49; H, 6.85; N, 3.52; S, 8.07. Found: C, 69.34; H, 6.67; N, 3.55; S, 8.15.

*Synthesis of Di-tert-butyl 1,4-Dioxo-3,6-di(thiophen-2-yl)pyrrolo-[3,4-c]pyrrole-2,5(1H,4H)-dicarboxylate (**8**).* Compound **8** was synthesized following the same procedure as that of compound **2** by using 3,6-di(thiophen-2-yl)pyrrolo[3,4-*c*]pyrrole-1,4(2*H*,5*H*)-dione (**7**) as the instead of compound **1** as the starting material. (0.80 g, 80%). ^{1}H NMR ($CDCl_3$, 600 MHz): 8.23 (d, J = 4.81 Hz, 1H), 7.63 (d, J = 4.96 Hz, 1H), 7.20 (t, J = 8.90 Hz, 1H), 1.59 (s, 9H). ^{13}C NMR ($CDCl_3$, 600 MHz): 159.04, 148.78, 137.92, 133.90, 131.80, 129.65, 128.06, 110.25, 85.91, 27.70. Anal. Calcd for $C_{24}H_{24}N_2O_6S_2$: C, 57.58; H, 4.83; N, 5.60; S, 12.81. Found: C, 57.72; H, 4.91; N, 5.54; S, 12.82.

*Synthesis of (E)-Di-tert-butyl-6,6′-bis(5-bromothiophen-2-yl)-3,3′-dioxo-[2,2′-biindolinylidene]-1,1′-dicarboxylate (**M1**).* To the solution of the compound **6** (1.0 g, 1.60 mmol) in THF (60 mL), *N*-bromosuccinimide (NBS) (0.683 g, 3.84 mmol) was added in five portions in 2 h at room temperature. After that, the mixture was stirred for another 4 h and then was poured into water. The organic phase was extracted with diethyl ether, washed by water, and dried over anhydrous magnesium sulfate. After the purification by silica chromatography with dichloromethane as the eluent, the product was obtained as brownish solid (1.06 g, 84%). ^{1}H NMR ($CDCl_3$, 600 MHz): 8.21 (s, 1H), 7.76 (d, J = 7.95 Hz, 1H), 7.37 (d, J = 9.56 Hz, 1H), 7.25 (d, J = 3.93 Hz, 1H), 7.10 (d, J = 4.10 Hz, 1H), 1.66 (s, 9H). ^{13}C NMR ($CDCl_3$, 600 MHz): 182.49, 149.81, 149.51, 144.72, 140.67, 131.45, 125.61, 125.43, 124.85, 122.07, 121.26, 114.35, 113.19, 84.82, 28.20. Anal. Calcd for $C_{34}H_{28}Br_2N_2O_6S_2$: C, 52.05; H, 3.60; N, 3.57; S, 8.18. Found: C, 52.51; H, 3.51; N, 3.62; S, 8.38.

*Synthesis of (E)-Di-tert-butyl 6,6′-bis(5-bromo-4-hexylthiophen-2-yl)-2,2′-dioxo-[3,3′-biindolinylidene]-1,1′-dicarboxylate (**M2**).* Compound **M2** was synthesized following the same procedure as that of compound **M1** by using compound **6** as the starting material. (1.76 g, 92%). ^{1}H NMR ($CDCl_3$, 600 MHz): 8.87 (d, J = 8.68 Hz, 1H), 8.12 (d, J = 1.67 Hz, 1H), 7.54 (m, J = 9.78 Hz,1H), 7.04 (s, 1H), 2.54 (t, J = 15.31 Hz, 2H), 1.65 (s, 9H), 1.52−1.47 (m, J = 14.41 Hz, 10H), 0.92 (m, J = 7.84 Hz, 3H). ^{13}C NMR ($CDCl_3$, 600 MHz): 165.38, 148.38, 141.95, 131.79, 130.19, 127.78, 127.31, 120.48, 117.89, 110.25, 108.78, 107.56, 85.54, 34.50, 32. 89. 28.10. Anal. Calcd for $C_{46}H_{52}Br_2N_2O_6S_2$: C, 57.78; H, 5.50; N, 2.94; S, 6.73. Found: C, 57.54; H, 5.77; N, 3.19; S, 6.92.

*Synthesis of Di-tert-butyl 3,6-Bis(5-bromothiophen-2-yl)-1,4-dioxopyrrolo[3,4-c]-pyrrole-2,5(1H,4H)-dicarboxylate (**M3**).* Compound **M3** was synthesized following the same procedure as that of compound **M1** by using compound **7** as the starting material. (1.19 g, 90.7%). ^{1}H NMR ($CDCl_3$, 600 MHz): 8.07 (d, J = 4.25 Hz, 1H), 7.15 (d, J = 4.22 Hz, 1H), 1.61 (s, 9H). ^{13}C NMR ($CDCl_3$, 600 MHz): 158.68, 148.80, 136.71, 134.47, 131.07, 130.91, 120.91, 110.30, 86.37, 27.76. Anal. Calcd for $C_{24}H_{22}Br_2N_2O_6S_2$: C, 43.78; H, 3.37; N, 4.25; S, 9.74. Found: C, 43.53; H, 3.37; N, 4.29; S, 9.78.

Synthesis of Copolymers. The general procedure to synthesize the copolymers: In a 25 mL dry flask, monomer **M4** (123.94 mg, 0.1 mmol), **M1** (**M2** or **M3**) (0.1 mmol) and $Pd_2(dba)_3$ (3 mg) and P(*o*-Tol)$_3$ (6 mg) were dissolved in degassed toluene (5 mL). The mixture was vigorously stirred at 100 °C under nitrogen for 12 h. After it was cooled to room temperature, the mixture was dropped into methanol. The polymer was precipitated and then collected by filtration. Then the polymer was washed in a Soxhlet extractor with acetone and hexane for 24 h sequentially. After that, the polymer was Soxhlet-extracted with chloroform. The chloroform fraction was collected and concentrated under reduced pressure, and which was then precipitated in methanol. The final product was collected by filtration and dried under vacuum at 40 °C overnight.

Synthesis of Boc-PBDT-I. Yield: 105.2 mg, 68.3%. ^{1}H NMR ($CDCl_3$, 600 MHz): 7.72 (s, 1H), 7.43 (d, 2H), 7.30 (d, 2H), 7.22 (s, 1H), 7.08 (s, 1H), 2.92 (t, 2H), 2.23 (t, 2H), 1.60 (s, 9H), 1.37−1.25 (m, 32H), 0.89 (m, 6H). Anal. Calcd for $C_{92}H_{118}N_2O_6S_6$: C, 71.74%; H, 7.72%; N, 1.82%; S, 12.49. Found: C, 72.12%; H, 7.99%; N, 1.87%; S, 12.54%. GPC: M_n = 34.8 kg mol^{-1}, M_w = 73.4 kg mol^{-1}, M_w/M_n = 2.11.

Synthesis of Boc-PBDT-II. Yield: 113.8 mg, 73.9%. ^{1}H NMR ($CDCl_3$, 600 MHz): 7.83 (m, 1H), 7.63 (d, 2H), 7.48 (m, 2H), 7.33 (d, 2H), 7.26 (s, 1H), 7.12 (s, 1H), 2.88 (t, 2H), 2.53 (t, 2H), 2.22 (t, 2H) 1.67 (s, 9H), 1.45−1.23 (m, 48H), 0.91 (m, 12H). Anal. Calcd for $C_{92}H_{118}N_2O_6S_6$: C, 71.74%; H, 7.72%; N, 1.82%; S, 12.49. Found: C, 71.33%; H, 7.81%; N, 1.79%; S, 12.43%. GPC: M_n = 24.3 kg mol^{-1}, M_w = 43.8 kg mol^{-1}, M_w/M_n = 1.80.

Synthesis of Boc-PBDT-DPP. Yield: 129.8 mg, 91.8%. ^{1}H NMR ($CDCl_3$, 600 MHz): 8.28 (s, 1H), 7.85 (s, 1H), 7.43 (m, 1H), 7.08 (m, 1H), 2.85 (t, 2H), 2.65 (t, 2H), 1.63 (s, 9H), 1.58−1.21 (m, 32H), 0.88 (m, 6H). Anal. Calcd for $C_{82}H_{112}N_2O_6S_6$: C, 69.64%; H, 7.98%; N, 1.98%; S, 13.60. Found: C, 69.33%; H, 7.76%; N, 1.85%; S, 13.91%. GPC: M_n = 33.7 kg mol^{-1}, M_w = 69.1 kg mol^{-1}, M_w/M_n = 2.05.

Measurement and Characterization. ^{1}H and ^{13}C NMR were characterized with Bruker-600 spectrometer operating at 600 MHz in deuterated chloroform solution at 298 K. Chemical shifts were recorded as δ values (ppm) with the internal standard of tetramethylsilane (TMS). Elemental Analysis is characterized with the instrument of Vario EL III. The number-average (M_n) and weight-average (M_w) molecular weights were determined with Waters GPC 2410 in THF using a calibration curve with standard polystyrene as a reference. Thermogravimetric analyses (TGA) were performed on a Netzsch TG 209 under nitrogen at a heating rate of 10 °C min^{-1}. Differential scanning calorimetry (DSC) was performed on a Netzsch DSC 204 under nitrogen flow at heating/cooling rates of 10/20 °C min^{-1}. FT-IR spectra were observed on a NEXUS 670 instrument. UV−vis absorption spectra were recorded on a HP 8453 spectrophotometer. Cyclic voltammetry (CV) was performed on a CHI600D electrochemical workstation with a glass carbon (GC) working electrode and a Pt wire counter electrode at a scanning rate of 50 mV s^{-1} against a saturated calomel electrode (SCE) as reference electrode with a nitrogen saturated anhydrous solution of tetra-*n*-butylammoniumhexafluorophosphate in acetonitrile (0.1 mol L^{-1}). Atomic force microscopy (AFM) measurements were carried out using a Digital Instrumental DI Multimode Nanoscope III in a taping mode. Polarized optical microscopy pictures were obained with a Nikon EclipssEgoo Pol instrument. Transmission electron microscopy (TEM) images were characterized with a JEM-2100F instrument.

FETs Fabrication and Characterization. To observe the hole mobility evolution of the copolymers with thermal cleavage treatment, FETs were fabricated in a top contact geometry using silver as source and drain electrode. Highly n-doped silicon and thermally grown silicon dioxide (300 nm) were used as the back gate and gate dielectric, respectively. Poly(methyl methacrylate) (PMMA) was then used for surface modification of the gate dielectric layer. The copolymer films (~60 nm) were spin-coated on PMMA treated substrates from 1,2-

DOI: 10.1021/am5089956
ACS Appl. Mater. Interfaces 2015, 7, 9038−9051

dichlorobenzene solution (10 mg/mL) at 2000 rpm, the films of copolymers with cleavage of *t*-Boc groups were obtained by applying annealing treatment at 200 °C for 10 min on the as-coated films. Then silver film (50 nm) was deposited under vacuum as the source and drain electrode. The width to length ratio (W/L) of the FET devices is 100/1. The device characterizations were performed in the atmosphere by using a probe station and a semiconductor parameter analyzer (Agilent 4155C). Then field effect mobility was calculated from the standard equation for saturation region in metal-dioxide-semiconductor field effect transistors: $I_{DS} = (W/2L)\mu C_i(V_G - V_T)^2$, where I_{DS} is the drain-source current, μ is the field-effect mobility, and C_i is the capacitance per unit area of the dielectric layer (C_i = 0.8× 10^{-8} nF cm^{-2}), V_G is the gate voltage, and V_T is the threshold voltage.

PSCs Fabrication and Characterization. Before fabrication of the solar cells, the indium tin oxide (ITO)-coated substrates were cleaned by ultrasonic treatment in deionized water, acetone, and isopropyl alcohol and then dried in a nitrogen stream. Polymer solar cells with inverted structures were fabricated with the structure of ITO/PFN-OX[50]/copolymer:$PC_{71}BM$/MoO_3/Al under conditions as follows: a 5 nm thick layer of PFN-OX was spin-coated on the ITO substrates and then the cross-linking process was done by heating the half-dried films under 150 °C for 20 min and fluorescence lamp illumination for 20 min.[50] The copolymer and $PC_{71}BM$ were codissolved in 1,2-dichlorobenzene with concentration of 10 mg mL^{-1}. All the active layers were then spin-coated from the prepared blending solutions with a thickness of 90 nm. To complete the device fabrication, 10 nm of MoO_3 and 100 nm of Al were subsequently thermally evaporated onto the active layer fo form the top electrode of the device. The effective device area was measured to be 0.16 cm^{-2}. The devices with the thermocleavaged copolymers were fabricated in similar procedures, just applying annealing treatment at 200 °C for 10 min on the as-coated active layer before the deposition of MoO_3 and cathode. The current density−voltage (J−V) characteristics were investigated with a Keithley 236 source meter.

■ ASSOCIATED CONTENT

Supporting Information

DSC scan curves in the first heating cycle of copolymers, electrochemical properties of polymers, HOMO and LUMO energy levels of copolymer unit based on DFT calculation, AFM, POM, and TEM images. This material is available free of charge via the Internet at http://pubs.acs.org.

■ AUTHOR INFORMATION

Corresponding Authors

*E-mail: msleiying@scut.edu.cn.
*E-mail: russell@mail.pse.umass.edu.
*E-mail: msfhuang@scut.edu.cn.

Notes

The authors declare no competing financial interest.

■ ACKNOWLEDGMENTS

The work was financially supported by the Ministry of Science and Technology (No. 2014CB643501), the Natural Science Foundation of China (No. 51303056, 21125419, 51323003, and 51361165301) and Guangdong Natural Science Foundation (Grant No. S2012030006232).

■ REFERENCES

(1) Kraft, A.; Grimsdale, A. C.; Holmes, A. B. Electroluminescent Conjugated Polymers-Seeing Polymers in a New Light. *Angew. Chem., Int. Ed.* **1998**, *37*, 402−428.

(2) Yu, G.; Gao, J.; Hummelen, J. C.; Wudl, F.; Heeger, A. J. Polymer Photovoltaic Cells: Enhanced Efficiencies via a Network of Internal Donor−Acceptor Heterojunctions. *Science* **1995**, *270*, 1789−1791.

(3) Akcelrud, L. Electroluminescent Polymers. *Prog. Polym. Sci.* **2003**, *28*, 875−962.

(4) Bao, Z.; Dodabalapur, A.; Lovinger, A. J. Soluble and Processable Regioregular Poly(3-Hexylthiophene) for Thin Film Field-Effect Transistor Applications with High Mobility. *Appl. Phys. Lett.* **1996**, *69*, 4108−4110.

(5) Glowacki, E. D.; Voss, G.; Demirak, K.; Havlicek, M.; Sunger, N.; Okur, A. C.; Monkowius, U.; Gasiorowski, J.; Leonat, L.; Sariciftci, N. S. A Facile Protection-Deprotection Route for Obtaining Indigo Pigments as Thin Films and Their Applications in Organic Bulk Heterojunctions. *Chem. Commun.* **2013**, *49*, 6063−6065.

(6) Zambounis, J. S.; Hao, Z.; Iqbal, A. Latent Pigments Activated by Heat. *Nature* **1997**, *388*, 131−132.

(7) Hodge, P.; A. Power, G.; A. Rabjohns, M. Synthesis of Poly(anthracene-2,6-diyl) and a Copolymer Containing Alternately Anthracene-2,6-diyl and P-phenylene Units. *Chem. Commun.* **1997**, *1*, 73−74.

(8) Uemura, T.; Mamada, M.; Kumaki, D.; Tokito, S. Synthesis of Semiconducting Polymers through Soluble Precursor Polymers with Thermally Removable Groups and Their Application to Organic Transistors. *ACS Macro Lett.* **2013**, *2*, 830−833.

(9) Liu, C.; Xu, W.; Guan, X.; Yip, H.-L.; Gong, X.; Huang, F.; Cao, Y. Synthesis of Anthracene-Based Donor−Acceptor Copolymers with a Thermally Removable Group for Polymer Solar Cells. *Macromolecules* **2014**, *47*, 8585−8593.

(10) Yu, J.; Holdcroft, S. Synthesis, Solid-Phase Reaction, and Patterning of Acid-Labile 3,4-Ethylenedioxythiophene-based Conjugated Polymers. *Chem. Mater.* **2002**, *14*, 3705−3714.

(11) Han, X.; Chen, X.; Holdcroft, S. Nanostructured Photovoltaic Devices from Thermally-Reactive π-Conjugated Polymer Blends. *Chem. Mater.* **2009**, *21*, 4631−4637.

(12) Jakob, S.; Moreno, A.; Zhang, X.; Bertschi, L.; Smith, P.; Schlüter, A. D.; Sakamoto, J. Synthesis of Polyphenylenes From a Soluble Precursor: The "Shaving" Approach. *Macromolecules* **2010**, *43*, 7916−7918.

(13) Bundgaard, E.; Hagemann, O.; Bjerring, M.; Nielsen, N. C.; Andreasen, J. W.; Andreasen, B.; Krebs, F. C. Removal of Solubilizing Side Chains at Low Temperature: A New Route to Native Poly(thiophene). *Macromolecules* **2012**, *45*, 3644−3646.

(14) Helgesen, M.; Gevorgyan, S. A.; Krebs, F. C.; Janssen, R. A. J. Substituted 2,1,3-Benzothiadiazole- and Thiophene-based Polymers for Solar Cells-Introducing a New Thermocleavable Precursor. *Chem. Mater.* **2009**, *21*, 4669−4675.

(15) Helgesen, M.; Bjerring, M.; Nielsen, N. C.; Krebs, F. C. Influence of the Annealing Temperature on the Photovoltaic Performance and Film Morphology Applying Novel Thermocleavable Materials. *Chem. Mater.* **2010**, *22*, 5617−5624.

(16) Liu, Y.; Scully, S. R.; McGehee, M. D.; Liu, J.; Luscombe, C. K.; Fréchet, J. M. J.; Shaheen, S. E.; Ginley, D. S. Dependence of Band Offset and Open-Circuit Voltage on the Interfacial Interaction Between TiO_2 and Carboxylated Polythiophenes. *J. Phys. Chem. B* **2006**, *110*, 3257−3261.

(17) Edder, C.; Armstrong, P. B.; Prado, K. B.; Frechet, J. M. J. Benzothiadiazole- and Pyrrole-Based Polymers Bearing Thermally Cleavable Solubilizing Groups as Precursors for Low Bandgap Polymers. *Chem. Commun.* **2006**, *1*, 1965−1967.

(18) Nielsen, C. B.; Sohn, E.-H.; Cho, D.-J.; Schroeder, B. C.; Smith, J.; Lee, M.; Anthopoulos, T. D.; Song, K.; McCulloch, I. Improved Field-Effect Transistor Performance of a Benzotrithiophene Polymer Through Ketal Cleavage in the Solid State. *ACS Appl. Mater. Interfaces* **2013**, *5*, 1806−1810.

(19) Duan, C.; Huang, F.; Cao, Y. Recent Development of Push-Pull Conjugated Polymers for Bulk-Heterojunction Photovoltaics: Rational Design and Fine Tailoring of Molecular Structures. *J. Mater. Chem.* **2012**, *22*, 10416−10434.

(20) Kroon, R.; Lenes, M.; Hummelen, J. C.; Blom, P. W. M.; De Boer, B. Small Bandgap Polymers for Organic Solar Cells. *Polym. Rev.* **2008**, *48*, 531−582.

DOI: 10.1021/am5089956
ACS Appl. Mater. Interfaces 2015, 7, 9038−9051

(21) Wang, E.; Mammo, W.; Andersson, M. R. 25th Anniversary Article: Isoindigo-based Polymers and Small Molecules for Bulk Heterojunction Solar Cells and Field Effect Transistors. *Adv. Mater.* **2014**, *26*, 1801−1826.
(22) Nielsen, C. B.; Turbiez, M.; McCulloch, I. Recent Advances in the Development of Semiconducting DPP-Containing Polymers for Transistor Applications. *Adv. Mater.* **2013**, *25*, 1859−1880.
(23) Głowacki, E. D.; Voss, G.; Leonat, L.; Irimia-Vladu, M.; Bauer, S.; Sariciftci, N. S. Indigo and Tyrian Purple-From Ancient Natural Dyes to Modern Organic Semiconductors. *Isr. J. Chem.* **2012**, *52*, 540−551.
(24) Chen, M.; Fu, W.; Shi, M.; Hu, X.; Pan, J.; Ling, J.; Li, H.; Chen, H. An Ester-Functionalized Diketopyrrolopyrrole Molecule with Appropriate Energy Levels for Application in Solution-Processed Organic Solar Cells. *J. Mater. Chem. A* **2013**, *1*, 105−111.
(25) Han, Y.; Chen, L.; Chen, Y. Diketopyrrolopyrrole-Based Liquid Crystalline Conjugated Donor−Acceptor Copolymers with Reduced Band Gap for Polymer Solar Cells. *J. Polym. Sci., Part A: Polym. Chem.* **2013**, *51*, 258−266.
(26) Bai, H.; Cheng, P.; Wang, Y.; Ma, L.; Li, Y.; Zhu, D.; Zhan, X. A Bipolar Small Molecule Based on Indacenodithiophene and Diketopyrrolopyrrole for Solution Processed Organic Solar Cells. *J. Mater. Chem. A* **2014**, *2*, 778−784.
(27) Xie, F.-X.; Choy, W. C. H.; Sha, W. E. I.; Zhang, D.; Zhang, S.; Li, X.; Leung, C.-W.; Hou, J. Enhanced Charge Extraction in Organic Solar Cells Through Electron Accumulation Effects Induced by Metal Nanoparticles. *Energy Environ. Sci.* **2013**, *6*, 3372−3379.
(28) Lee, J.; Han, A. R.; Hong, J.; Seo, J. H.; Oh, J. H.; Yang, C. Inversion of Dominant Polarity in Ambipolar Polydiketopyrrolopyrrole with Thermally Removable Groups. *Adv. Funct. Mater.* **2012**, *22*, 4128−4138.
(29) Liang, Y. Y.; Feng, D. Q.; Wu, Y.; Tsai, S. T.; Li, G.; Ray, C.; Yu, L. P. Highly Efficient Solar Cell Polymers Developed via Fine-Tuning of Structural and Electronic Properties. *J. Am. Chem. Soc.* **2009**, *131*, 7792−7799.
(30) Huo, L.; Hou, J.; Zhang, S.; Chen, H.-Y.; Yang, Y. A Polybenzo[1,2-B:4,5-Bu,Dithiophene Derivative with Deep HOMO Level and its Application in High-Performance Polymer Solar Cells. *Angew. Chem., Int. Ed.* **2010**, *49*, 1500−1503.
(31) Huo, L.; Zhang, S.; Guo, X.; Xu, F.; Li, Y.; Hou, J. Replacing Alkoxy Groups with Alkylthienyl Groups: A Feasible Approach to Improve the Properties of Photovoltaic Polymers. *Angew. Chem., Int. Ed.* **2011**, *50*, 9697−9702.
(32) Zhan, X.; Zhu, D. Conjugated Polymers for High-Efficiency Organic Photovoltaics. *Polym. Chem.* **2010**, *1*, 409−419.
(33) Tanoue, Y.; Terada, A.; Sakata, K.; Hashimoto, M.; Morishita, S.-I.; Hamada, M.; Kai, N. A Facile Synthesis of Tyrian Purple Based on a Biosynthetic Pathway. *Fish. Sci.* **2001**, *67*, 726−729.
(34) Sun, B.; Hong, W.; Aziz, H.; Li, Y. Diketopyrrolopyrrole-Based Semiconducting Polymer Bearing Thermocleavable Side Chains. *J. Mater. Chem.* **2012**, *22*, 18950−18955.
(35) Chen, S.; Sun, B.; Hong, W.; Yan, Z.; Aziz, H.; Meng, Y.; Hollinger, J.; Seferos, D. S.; Li, Y. Impact of N-Substitution of a Carbazole Unit on Molecular Packing and Charge Transport of DPP-Carbazole Copolymers. *J. Mater. Chem. C* **2014**, *2*, 1683−1690.
(36) Irimia-Vladu, M.; Głowacki, E. D.; Troshin, P. A.; Schwabegger, G.; Leonat, L.; Susarova, D. K.; Krystal, O.; Ullah, M.; Kanbur, Y.; Bodea, M. A.; Razumov, V. F.; Sitter, H.; Bauer, S.; Sariciftci, N. S. Indigo—A Natural Pigment for High Performance Ambipolar Organic Field Effect Transistors and Circuits. *Adv. Mater.* **2012**, *24*, 375−380.
(37) Brabec, C. J.; Winder, C.; Sariciftci, N. S.; Hummelen, J. C.; Dhanabalan, A.; van Hal, P. A.; Janssen, R. A. J. A Low-Bandgap Semiconducting Polymer for Photovoltaic Devices and Infrared Emitting Diodes. *Adv. Funct. Mater.* **2002**, *12*, 709−712.
(38) Pommerehne, J.; Vestweber, H.; Guss, W.; Mahrt, R. F.; Bässler, H.; Porsch, M.; Daub, J. Efficient Two Layer Leds on a Polymer Blend Basis. *Adv. Mater.* **1995**, *7*, 551−554.
(39) Frisch, M. J.; Trucks, G. W.; Schlegel, H. B.; Scuseria, G. E.; Robb, M. A.; Cheeseman, J. R.; Scalmani, G.; Barone, V.; Mennucci, B.; Petersson, G. A.; Nakatsuji, H.; Caricato, M.; Li, X.; Hratchian, H. P.; Izmaylov, A. F.; Bloino, J.; Zheng, G.; Sonnenberg, J. L.; Hada, M.; Ehara, M.; Toyota, K.; Fukuda, R.; Hasegawa, J.; Ishida, M.; Nakajima, T.; Honda, Y.; Kitao, O.; Nakai, H.; Vreven, T.; Montgomery, J. A., Jr.; Peralta, J. E.; Ogliaro, F.; Bearpark, M.; Heyd, J. J.; Brothers, E.; Kudin, K. N.; Staroverov, V. N.; Kobayashi, R.; Normand, J.; Raghavachari, K.; Rendell, A.; Burant, J. C.; Iyengar, S. S.; Tomasi, J.; Cossi, M.; Rega, N.; Millam, J. M.; Klene, M.; Knox, J. E.; Cross, J. B.; Bakken, V.; Adamo, C.; Jaramillo, J.; Gomperts, R.; Stratmann, R. E.; Yazyev, O.; Austin, A. J.; Cammi, R.; Pomelli, C.; Ochterski, J. W.; Martin, R. L.; Morokuma, K.; Zakrzewski, V. G.; Voth, G. A.; Salvador, P.; Dannenberg, J. J.; Dapprich, S.; Daniels, A. D.; Farkas, O.; Foresman, J. B.; Ortiz, J. V.; Cioslowski, J.; Fox, D. J. *Gaussian 09*; Gaussian, Inc.: Wallingford, CT, 2009.
(40) Deman, A. L.; Tardy, J. PMMA−Ta_2O_5 Bilayer Gate Dielectric for Low Operating Voltage Organic FETs. *Org. Electron.* **2005**, *6*, 78−84.
(41) Shi, W.; Yu, J.; Huang, W.; Yu, X.; Zheng, Y. Performance Enhancement of Poly(3-hexylthiophene) Organic Field-Effect Transistor by Inserting Poly(Methylmethacrylate) Buffer Layer. *Appl. Phys. Lett.* **2013**, *102*, 111607−111612.
(42) She, X.-J.; Liu, J.; Zhang, J.-Y.; Gao, X.; Wang, S.-D. Operational Stability Enhancement of Low-Voltage Organic Field-Effect Transistors Based on Bilayer Polymer Dielectrics. *Appl. Phys. Lett.* **2013**, *103*, 133303−133309.
(43) Noh, Y.-Y.; Zhao, N.; Caironi, M.; Sirringhaus, H. Downscaling of Self-Aligned, All-Printed Polymer Thin-Film Transistors. *Nat. Nanotechnol.* **2007**, *2*, 784−789.
(44) Chen, Z.; Cai, P.; Chen, J.; Liu, X.; Zhang, L.; Lan, L.; Peng, J.; Ma, Y.; Cao, Y. Low Band-Gap Conjugated Polymers with Strong Interchain Aggregation and Very High Hole Mobility Towards Highly Efficient Thick-Film Polymer Solar Cells. *Adv. Mater.* **2014**, *26*, 2586−2591.
(45) Minari, T.; Liu, C.; Kano, M.; Tsukagoshi, K. Controlled Self-Assembly of Organic Semiconductors for Solution-Based Fabrication of Organic Field-Effect Transistors. *Adv. Mater.* **2012**, *24*, 299−306.
(46) Gamerith, S.; Klug, A.; Scheiber, H.; Scherf, U.; Moderegger, E.; List, E. J. W. Direct Ink-Jet Printing of Ag−Cu Nanoparticle and Ag-Precursor Based Electrodes for OFET Applications. *Adv. Funct. Mater.* **2007**, *17*, 3111−3118.
(47) Fukuda, K.; Sekine, T.; Kobayashi, Y.; Kumaki, D.; Itoh, M.; Nagaoka, M.; Toda, T.; Saito, S.; Kurihara, M.; Sakamoto, M.; Tokito, S. Stable Organic Thin-Film Transistors Using Full Solution-Processing and Low-Temperature Sintering Silver Nanoparticle Inks. *Org. Electron.* **2012**, *13*, 1660−1664.
(48) Zhong, C.; Liu, S.; Huang, F.; Wu, H.; Cao, Y. Highly Efficient Electron Injection from Indium Tin Oxide/Cross-Linkable Amino-Functionalized Polyfluorene Interface in Inverted Organic Light Emitting Devices. *Chem. Mater.* **2011**, *23*, 4870−4876.
(49) Zhuang, W.; Bolognesi, M.; Seri, M.; Henriksson, P.; Gedefaw, D.; Kroon, R.; Jarvid, M.; Lundin, A.; Wang, E.; Muccini, M.; Andersson, M. R. Influence of Incorporating Different Electron-Rich Thiophene-Based Units on the Photovoltaic Properties of Isoindigo-Based Conjugated Polymers: An Experimental and DFT Study. *Macromolecules* **2013**, *46*, 8488−8499.
(50) Liu, S.; Zhong, C.; Zhang, J.; Duan, C.; Wang, X.; Huang, F. A Novel Crosslinkable Electron Injection/Transporting Material for Solution Processed Polymer Light-Emitting Diodes. *Sci. China Chem.* **2011**, *54*, 1745−1749.
(51) McNeill, C. R.; Westenhoff, S.; Groves, C.; Friend, R. H.; Greenham, N. C. Influence of Nanoscale Phase Separation on the Charge Generation Dynamics and Photovoltaic Performance of Conjugated Polymer Blends: Balancing Charge Generation and Separation. *J. Phys. Chem. C* **2007**, *111*, 19153−19160.
(52) Heeger, A. J. 25th Anniversary Article: Bulk Heterojunction Solar Cells: Understanding the Mechanism of Operation. *Adv. Mater.* **2014**, *26*, 10−28.
(53) Zhang, Y.; Yip, H.-L.; Acton, O.; Hau, S. K.; Huang, F.; Jen, A. K. Y. A Simple and Effective Way of Achieving Highly Efficient and

DOI: 10.1021/am5089956
ACS Appl. Mater. Interfaces 2015, 7, 9038−9051

Thermally Stable Bulk-Heterojunction Polymer Solar Cells Using Amorphous Fullerene Derivatives as Electron Acceptor. *Chem. Mater.* **2009**, *21*, 2598−2600.
(54) Wang, E.; Ma, Z.; Zhang, Z.; Vandewal, K.; Henriksson, P.; Inganäs, O.; Zhang, F.; Andersson, M. R. An Easily Accessible Isoindigo-based Polymer for High-Performance Polymer Solar Cells. *J. Am. Chem. Soc.* **2011**, *133*, 14244−14247.
(55) Stalder, R.; Mei, J.; Reynolds, J. R. Isoindigo-Based Donor−Acceptor Conjugated Polymers. *Macromolecules* **2010**, *43*, 8348−8352.
(56) Liu, S.; Zhang, Z.; Chen, D.; Duan, C.; Lu, J.; Zhang, J.; Huang, F.; Su, S.; Chen, J.; Cao, Y. Synthesis and Optoelectronic Properties of Amino-Functionalized Carbazole-Based Conjugated Polymers. *Sci. China Chem.* **2013**, *56*, 1119−1128.

DOI: 10.1021/am5089956
ACS Appl. Mater. Interfaces 2015, 7, 9038−9051